Structure and Identity of 4,4′-Thiobisbenzenethiol Self-Assembled Monolayers

Yuling Wang,[†,‡] Linfeng Gan,[†,‡] Hongjun Chen,[†,‡] Shaojun Dong,[*,‡] and Jin Wang[*,§]

State Key Laboratory of Electroanalytical Chemistry, Changchun Institute of Applied Chemistry, Chinese Academy of Sciences, Changchun 130022, Jilin, People's Republic of China, Graduate School of the Chinese Academy of Sciences, Beijing, 100039, People's Republic of China, and Department of Chemistry, State University of New York at Stony Brook, New York 11794-3400

Received: April 20, 2006; In Final Form: August 5, 2006

Self-assembled monolayers (SAMs) of 4,4′-thiobisbenzenethiol (TBBT) can be formed on Au surface spontaneously. The structural characteristics and adsorption behavior of TBBT SAMs on Au have been investigated by surface enhanced Raman scattering (SERS), electrochemical cyclic voltammetry (CV), ac impedance spectroscopy (EIS), and atomic force microscopy (AFM). It is demonstrated that TBBT adsorbed on Au by losing a H atom, forming one Au−S bond, and the other mercapto group is free at the surface of the monolayer owing to the presence of the ν_{S-H} at 2513 cm^{-1} and the δ_{C-S-H} at 910 cm^{-1} in SERS. The enhancement of the vibration of C−S (1064 cm^{-1}), the aromatic C−H vibration (3044 cm^{-1}), and the absence of the vibration of S−S illustrate TBBT adsorbed on Au forming a monolayer with one benzene ring tilted with respect to the Au surface. The interpretation of the observed frequencies is aided by ab initio molecular orbital (MO) calculations at the HF/6-31G* level of theory. Electrochemical CV and EIS indicate TBBT monolayers can passivate the Au effectively for its low ratio of pinhole defects ($\theta = 99.6\%$). AFM studies give details about the surface morphology. The applications of TBBT SAMs have been extensively investigated by exposure of Cu^{2+} ion to TBBT SAMs on Au and covalent adsorption of metal nanoparticles. Electrochemical, X-ray photoelectron spectroscopic, and SERS results indicate that Cu^{2+} can react with TBBT SAMs and present on TBBT SAMs as Cu(I). A scanning electron microscopic image of Ag nanoparticles on TBBT/Au and the Raman spectrum of TBBT in smooth macroscopic Au/TBBT SAMs/Ag nanoparticle sandwich structure indicate that metal nanoparticles can be adsorbed on TBBT SAMs effectively through covalent linkage.

Introduction

Self-assembled monolayers (SAMs) have attracted a lot of attention in past decades owing to their ability to form organized, well-packed, and crystalline-like assemblies on surfaces.[1] Thiols are the first and most frequent system to be particularly well studied on Au and Ag and are used as model systems for a wide variety of applications ranging from corrosion,[2] lubrication and adhesion,[3] and biomaterial and biosensor surfaces[4] to the area of nanotechnology.[5] Among the thiols, alkanethiols adsorbed on Au are the most extensively studied SAMs because of their stability and high degree of organization.[6] In addition to aliphatic thiols, aromatic thiol monolayers have been studied recently because of their highly delocalized electron density and structural rigidity of the phenyl ring and their potential applications in charge transfer and electronic functionality.[7] There have been some research on aromatic thiol monolayers on Au.[8−11] Rubinstein and co-workers have investigated aromatic thiol monolayers such as thiophenol, *p*-biphenyl mercaptan, and *p*-terphenyl mercaptan on Au by contact angle (CA) measurement, ellipsometry, electrochemical cyclic voltammetry (CV), and ac impedance spectroscopy (EIS) to find that the blocking efficiency is increased with the number of phenyl rings in the molecule.[8] Ganesh et al. have studied SAMs of 2-naphthalenethiol on Au by scanning tunneling microscopy (STM), Fourier transform infrared (FT-IR) spectroscopy, and electrochemistry.[9] Their results indicated that 2-naphthalenethiol on Au forms a stable and reproducible, but moderately blocking, monolayer. Käfer et al. have carried out a comprehensive study of SAMs of anthracenethiol on Au and have shown that the saturated monolayer is stable and inert under ambient conditions, while the dilute phase does not warrant any protection of the sulfur headgroups which oxidize rapidly in air.[10] Our group has also investigated the SAMs of thiophene derivatives on Au by electrochemical method.[11] The studies on SAMs of 2-mercapto-3-*n*-octylthiophene (MOT) on Au indicate that the MOT monolayers on the electrode can provide an excellent barrier for hydrated ionic probe penetration but cannot accommodate the organic species penetration effectively, providing a more energetically favorable hydrophobic surface for the addition of phospholipid vesicles.[11a]

Because SAMs have well-organized, packed properties and stability, they can be characterized by various physical methods such as CA, ellipsometry, X-ray photoelectron spectroscopy (XPS), surface enhanced Raman scattering (SERS), STM, FT-IR, and quartz crystal microscopy (QCM). Among these SERS spectroscopy is a powerful tool in surface chemistry owing to its high sensitivity and selectivity in providing useful information regarding metal−adsorbate interfaces. The adsorption behavior and orientation of the adsorbate on metal can be determined based on the relative intensity and position of the bands in SERS spectra. Pemberton and co-workers have investi-

* Corresponding authors. Telephone: 86-431-5262101 (S.D.); (631) 827-9971 (J.W.). Fax: +86-431-5689711 (S.D.); (631) 756-6926 (J.W.). E-mail: dongsj@ciac.jl.cn (S.D.); jin.wang.1@stonybrook.edu (J.W.).

† Changchun Institute of Applied Chemistry, Chinese Academy of Sciences.

‡ Graduate School of the Chinese Academy of Sciences.

§ State University of New York at Stony Brook.

10.1021/jp062422m CCC: $33.50
Published on Web 09/21/2006

gated self-assembled monolayer films of alkanethiol on Ag and Au by SERS and proposed the surface selection rules for Raman spectroscopy used to estimate the orientation of alkanethiol layer on Au.[12] In addition to alkanethiol, they also reported monolayer films of thiophenol and 4-mercaptopyridine on Pt and demonstrated the feasibility of studying surface chemistry using Raman spectroscopy.[13] Kim and co-workers have reported systematic investigations on the adsorption of dithiol including alkanedithiols and aromatic dithiol by SERS.[14] All these studies have successfully used the SERS technique to give the characteristics of SAMs on Ag or Au. Therefore, SERS is an effective technique to characterize the monolayers on metal surfaces. Chemical methods used are mainly electrochemical CV and EIS, which are especially effective for testing the quality of the SAMs and simultaneously giving information about packing density, surface coverage, distribution of pinholes, and defects in the formation of SAMs.

To the best of our knowledge, there is no report in the literature on the normal Raman spectrum of 4,4′-thiobisbenzenethiol (TBBT) and its adsorption on Au surface. In this paper, we first investigate the minimized geometry of neutral TBBT and give the assignments of its Raman spectrum based on ab initio molecular orbital (MO) calculations at the HF/6-31G* level of theory. Its orientation on Au surface, the surface coverage, the distribution of pinholes, and the surface morphology of TBBT SAMs on Au are estimated by SERS, electrochemical CV, EIS, and atomic force microscopy (AFM). Because of the structural properties of TBBT SAMs on Au, it is assumed that it may be useful to react them with metal ion forming metal functionalized bilayer or multilayer films and covalently adsorb metal nanoparticles to form two- or three-dimensional (2D or 3D) nanostructures, which have great significance for applications in molecular electronic devices.

The aim of the present investigation is 2-fold: first, to describe the structural properties of TBBT SAMs on Au and, second, to test the applications of TBBT SAMs to react with metal ion and covalently adsorb metal nanoparticles.

Experimental Section

Materials. 4,4′-Thiobisbenzenethiol (TBBT), potassium ferricyanide, trisodium citrate, $AgNO_3$, and $CuCl_2$ were all obtained from Aldrich and used without further purification. All other reagents were of analytical grade and were used also without further purification. Milli-Q grade water (>18 MΩ) was used for all solution preparation and experiments.

Sample Preparation. The Au electrode, subjected to the following pretreatment procedure, was polished with 0.3 μm α-Al_2O_3 and washed ultrasonically with water. Before chemical modification, the electrode was cleaned in 0.5 M H_2SO_4 by potential scanning between 0 and 1.5 V until a reproducible CV was obtained. After cleaning, the electrode was rinsed with deionized water and ethanol and immediately immersed into ethanol solutions containing 0.1 mM TBBT at room temperature for 24 h to form the monolayer. The monolayer film electrode was removed from the solution and carefully rinsed with pure ethanol and blown dry with argon.

Au substrates used for SERS measurement were prepared using a traditional double-potential step oxidation−reduction cycle (ORC) in 0.1 M KCl solutions as described in the literature.[15a] The Ag colloid solution was prepared by reducing $AgNO_3$ with citrate according to the protocol reported.[16] Au substrates used for AFM measurements were prepared according to a procedure by Chen et al.[15c]

Instruments. Electrochemical experiments were carried out on an Autolab PGSTAT 30 potentiostat (Utrecht, The Netherlands) in a conventional one-compartment cell. The cell was housed in a homemade Faraday cage to reduce stray electrical noise. All measurements were performed using a standard three-electrode system. A Ag/AgCl electrode was used as the reference electrode, Pt foil was used as the counter electrode, and the Au plate (0.8 mm in diameter) or SAMs on Au was used as the working electrode.

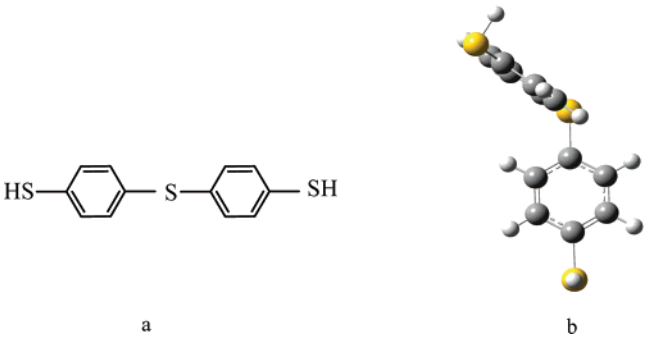

Figure 1. Molecular structure of TBBT (a) and HF/6-31G* optimized structure of neutral TBBT (b).

FT-Raman and FT-SERS spectra were conducted on Nicolet-960 FT-Raman spectrometer equipped with an InGaAs detector and a Nd/VO_4 laser (1064 nm) as an excitation source. The resolution of the Raman instrument was ca. 4 cm^{-1} at the excitation wavelength used here; the laser power used was about 300 mW and the scattered light was collected in a 180° geometry. All FT-Raman and FT-SERS were recorded by averaging 256 scans.

Raman and SERS spectra were recorded with a T64000 Raman spectrometer equipped with an integral microscope and a liquid nitrogen cooled charge-coupled device (CCD) camera. Radiation of 514.5 nm was from an Ar^+ ion laser. With a holographic grating (1800 grooves/mm) and a 50 μm slit, a spectral resolution of 1 cm^{-1} can be obtained. A silicon wafer with a Raman band at 520 cm^{-1} was used to calibrate the spectrometer. All of the Raman spectra were recorded in 10 s.

Tapping-mode AFM was conducted with a SPI3800N microscope instrument (Seiko Instruments, Inc.) on Au(111) facet of a gold bead electrode.

XPS measurements were performed on an ESCLAM MKII (VG Co., U.K.), using Mg as the exciting source. The operating pressure in the analysis chamber was below 10^{-9} Torr with the analyzer pass energy of 50 eV.

SEM imaging of Ag nanoparticles on TBBT/Au was conducted on an XL30 ESEM FEG field emission scanning electron microscopy (FEI Company).

Computation Methods. Ab initio molecular orbital (MO) calculations were performed using the Gaussian 03 program[17a] following geometry optimization with the 6-31G* basis set,[17b] and a scaling factor of 0.8929 was used for the calculation. All the molecular parameters in the C_1 symmetry were optimized; optimized parameters were used for the final frequency calculation.

Results and Discussion

The Structure of TBBT SAMs on Au. *Raman and SERS Studies.* Raman and SERS spectra of TBBT have been carried out to characterize its structure and orientation on Au surface. The TBBT molecule has a peculiar molecular structure that consists of two mercapto groups and two benzene rings, which are linked by a S atom as shown in Figure 1a. To the best of our knowledge, no Raman spectrum of this molecule has yet been studied. To interpret the obtained Raman spectrum, ab

TABLE 1: Peak Positions (in cm^{-1}) and Assignments of the Normal Raman (NR) Spectrum of TBBT and SERS Spectrum of TBBT on Au, and Scaled[a] 6-31G* Frequencies (in cm^{-1})

NR	SERS	6-31G(d) freq neu[b]	assignment[c]
3053	3044	3036	ν_{CH}(arom)
2554	2513	2580	ν_{SH}
1576	1570	1601	$\nu_{CC} + \nu_{CH}$
1186	1176	1180	ω_{CH}
1078	1064	1070	ν_{CS}
919	910	936	δ_{CSH}
735	741	730	ν_{asCSC}
704	699	705	ν_{sCSC}
628	629	619	
555	546	543	
491	488	491	

[a] Multiplied by 0.8929. [b] Neutral molecule. [c] From refs 14, 20, and 24c.

initio MO calculations were performed at the HF/6-31G* level on the TBBT molecule. The optimized geometry of neutral TBBT as indicated in Figure 1b gives a molecular structure of C_1 point group symmetry and dipole moment of 1.433 D. The two benzene rings are not in a line with each other but have an angle with 110° according to the calculated optimized neutral geometry, which corresponds to the results reported by Santo et al., who investigated the adsorption of TBBT on Ag(111) by second harmonic generation (SHG).[18] The Raman frequencies were calculated and the assignments were obtained as listed in Table 1; the scaling factor of 0.8929 was used for the calculation.

Curve a in Figure 2 gives the normal Raman spectrum of solid TBBT. The vibrations at 3053, 2554, 1576, 1186, 1078, 919, 735, and 704 cm^{-1} are in good agreement with calculated frequencies, which are assigned to the stretching vibration of aromatic C−H (ν_{CH}), the stretching vibration of S−H (ν_{SH}), the framework vibration of the aromatic ring ($\nu_{CC} + \nu_{CH}$), the wag of C−H (ω_{CH}), the stretching vibration of C−S (ν_{CS}), the deformation vibration of C−S−H (δ_{CSH}), the antisymmetric stretching vibration of (ν_{asCSC}), and the symmetric stretching vibration of C−S−C (ν_{sCSC}), respectively. It is worth noting that, at low frequencies, there are some Raman peaks, which were assigned to the vibrations with contributions from the aromatic C−H and C−S. Curve b in Figure 2 shows the SERS spectrum of TBBT coated on Au surface, which resembles the normal Raman spectrum of solid TBBT. The absence of the vibration of S−S at about 505 cm^{-1} indicates TBBT adsorbed on Au surface forming a monolayer, which is similar to that reported by Kim and co-workers.[14] The chemisorptions of Au−S can be manifested by the enhancement of the ν_{C-S} at 1064 cm^{-1} according to the surface selection rule[19] and the downshift of the frequency of the C−S mode on Au, which is shifted from 1078 to 1064 cm^{-1}. From the SERS spectrum of TBBT on Au surface, the ν_{S-H} at 2513 cm^{-1} and the deformation vibration of C−S−H (δ_{CSH}) at 910 cm^{-1} can be observed clearly although very weakly, which suggests that TBBT should bind to Au to form only one Au−S bond and the other S−H is free at the surface of the monolayer.

Comparing with the normal Raman spectrum of TBBT, the position and intensity of the vibration of S−H in SERS change greatly. This phenomenon is also present in the system of 1,3-propanedithiol (PDT) on Au reported by Joo et al.,[14c,d] who investigated the adsorption characteristics of PDT on a colloid Au surface. They obtained the weak enhancement of ν_{S-H} at 2512 cm^{-1} and inferred that the weak enhancement might derive from the long distance and parallel orientation of the S−H to the Au surface, and they attributed the frequency shifts to the formation of the hydrogen bonds. Thus, in our system we propose that the great change in intensity and frequency of S−H compared with the normal Raman spectrum of TBBT may be derived from two causes: first, the weak intensity may be attributed to the long distance of the S−H from the Au surface and the rather parallel orientation of the S−H bond with respect to the Au, which produces weak enhancement according to the surface selection rules.[19] Second, the very substantial frequency shift from 2554 to 2513 cm^{-1} by 41 cm^{-1} may indicate that the S−H group interacts with other S−H groups by forming hydrogen bonds. The vibration of the aromatic C−H at 3053 cm^{-1} is downshifted to 3044 cm^{-1}, which is a vibration mode to be used to determine the orientation of a molecule on the metals,[19] indicative of the benzene ring being tilted with the Au surface.[19c] However, the intensity is not very intense, which is attributed to the long distance of the other benzene ring from the Au surface and the slight tilt with the Au surface.

From the above discussion, it was demonstrated that TBBT adsorbed on Au surface forms a monolayer with one benzene ring tilted to the Au surface with a slight angle, while the other benzene ring tilts to the Au surface with an angle of 110°. It should be noted that the 110° was obtained according to the ab initio geometry optimization (the angle between the two phenyl groups is 110°). Because S between the two phenyl groups presents a sp^3 hybridization, the angle between the two phenyl groups must be about 110°, which is accordance with the reports by Santos.[18a] The presence of ν_{S-H} at 2513 cm^{-1} indicates that the Au surface is mercapto surplus. It should be mentioned that Kim and co-workers have proposed that aromatic sulfides on Ag can dissociate into phenyl thiol under 514.5 nm excitation,[20] while in our system, under 1064 nm excitation, TBBT is not dissociated to phenyl thiol because of the presence of the antisymmetric stretching vibration of ν_{asCSC} at 741 cm^{-1} and the symmetric stretching vibration of C−S−C (ν_{sCSC}) at 699 cm^{-1}, respectively.

Electrochemical Studies. To demonstrate the barrier properties to the probe and the surface coverage and distribution of pinholes on TBBT SAMs, electrochemical CV and EIS have been performed. Figure 3 shows the CV curves at the bare Au electrode and TBBT SAMs coated Au electrode in 5 mM $Fe(CN)_6^{3-}$ with 0.1 M KCl as the supporting electrolyte, with a scan rate of 50 mV/s. At the bare Au electrode, the shape of the CV curve and the peak separation of 60 mV are indicative of a diffusion-limited or electrochemically quasi-reversible one-electron redox process.[21] The CV curve at the TBBT coated Au electrode is markedly different from that at the bare Au electrode. The electron transfer has been fully inhibited. To clearly see the electrochemical behavior of TBBT SAMs on the Au electrode, Figure 3b was enlarged 10-fold as shown in Figure 3c. Obviously, the shape of the CV curve at the TBBT coated Au electrode has greatly changed: no peaks were observed, indicating that the monolayer can passivate the gold electrode surface effectively.

Electrochemical impedance spectroscopy is an effective method to anticipate pinholes or the coverage of the SAMs on the Au electrode because it is performed at very low overpotentials.[21] From the CV curves at the TBBT coated Au electrode, we have seen that $Fe(CN)_6^{3-}$ species cannot approach and exchange electrons with the underlying Au electrode, indicating that TBBT monolayer can block the electron-transfer reactions between $Fe(CN)_6^{3-}$ and the Au electrode. Thus $Fe(CN)_6^{3-/4-}$ can be suitable used as a redox couple probe for EIS measurement to determine the parameters of the pinholes within the SAMs. Figure 4 shows the EIS of TBBT monolayer coated Au

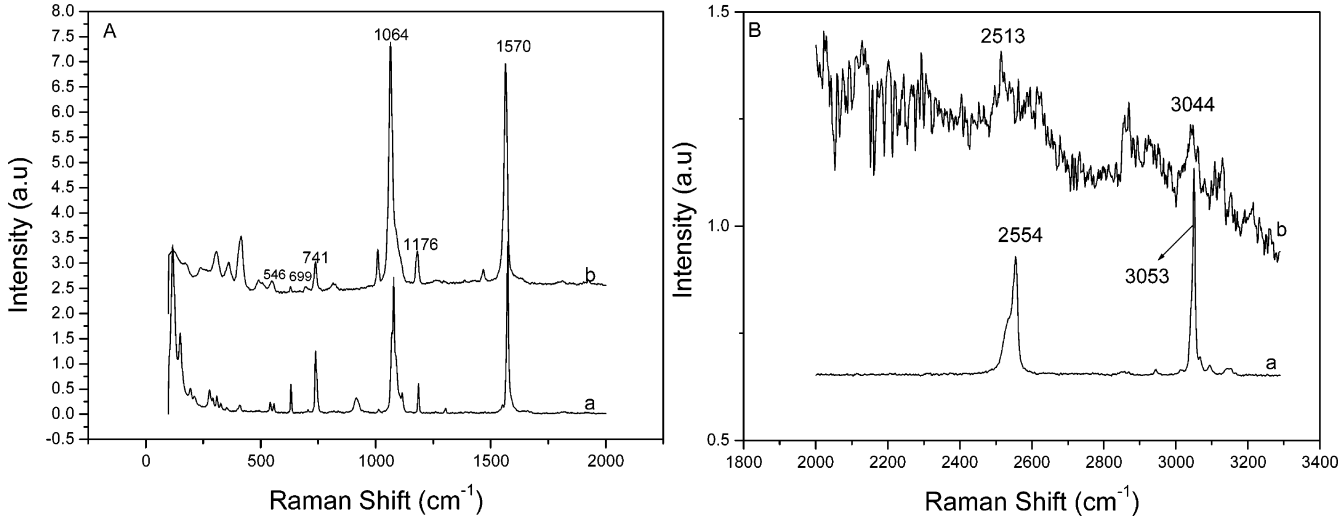

Figure 2. FT-Raman spectra of (a) solid TBBT and (b) TBBT monolayers coated on Au. (A) Spectra from 100 to 1800 cm^{-1} and (B) the expanded C−H and S−H stretching region (from 2000 to 3300 cm^{-1}).

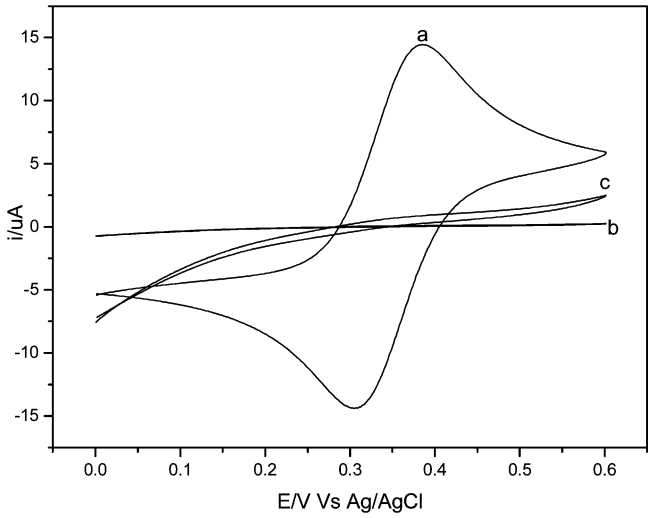

Figure 3. Cyclic voltammetric current response versus applied potential for the bare Au electrode (a) and TBBT coated Au electrode (b and c) in 5 mM potassium ferrocyanide with 0.1 M KCl as the supporting electrolyte at potential scan rate of 50 mV/s. Curve c is a 10-fold enlargement of curve b to clearly show the electrochemical behavior of TBBT on Au electrode.

electrode compared to the case of the bare Au electrode. In Figure 4A, a straight line at low frequency and a small semicircle at a high-frequency region can be observed, demonstrating that the process is essentially diffusion-controlled for the redox couple on the bare electrode, corresponding to the results of CV on bare Au electrode shown in Figure 3a. Figure 4B gives the EIS of TBBT coated Au electrode with a large semicircle at high frequency. According to Randle's equivalent circuit, two frequency regions can be distinguished to understand the effect of the monolayer on the response of the electroactive species at the electrode/SAM/electrolyte interface.[22,23] Rubinstein and co-workers have proposed a relative simple method to estimate the coverage of the SAMs on an electrode.[23] As reported by Peng et al.,[11] it is easy to relate the magnitude of R_{ct} to the coverage of the electrode by assuming that electron-transfer reactions occur only at bare spots on the electrode surface and that the diffusion to pinhole sites is planar. On the basis of the assumption, the apparent fractional coverage (θ) of the electrode based on the R_{ct} of the uncoated electrode can be obtained to be $\theta = 1 - R_{ct}^{bare}/R_{ct}^{SAMs}$, where θ is the coverage fraction of the electrode and R_{ct}^{bare} and R_{ct}^{SAMs} are the values of the charge-transfer resistances before and after electrode functionalization. From the EIS in Figure 4, we can calculate the charge-transfer resistances of about 6 Ω cm^2 for the bare Au electrode and 1400 Ω cm^2 for the TBBT SAMs/Au electrode. Then the apparent surface coverage (θ) can be estimated as approximately 99.6%, which indicates that a low ratio of pinholes existed with the SAMs on the Au electrode.

AFM Studies. The surface structure and morphology of the gold substrate have been characterized by AFM as shown in Figure 5B,C, which exhibits a clustered surface morphology, with irregularly shaped islands covering the surface measuring from 1 to 5 nm in width, greatly different from that bare Au(111) surface as shown in Figure 5A. Zooming in to view the surface as shown in Figure 5C indicates surface roughness of about 0.5 nm, which demonstrates the monolayer of TBBT SAMs on Au surface, corresponding to the results reported by Brower et al.,[24a,b] who investigated the morphology of 4,4′-dimercaptobiphenyl SAMs on Au surface.

Applications for TBBT SAMs on Au. Figure 6 shows the scheme of the orientation of TBBT SAMs on Au and its potential application in reaction with metal ion and covalent adsorption of metal nanoparticles. According to the discussion above, it has been shown that TBBT adsorbed on Au surface by losing a H atom forming one Au−S bond, while the other thiol group is free at the surface with one of the benzene rings slightly tilted with the surface. The free S−H group at the monolayer can react with metal ions, which leads to the formation of a metal ion functional bilayer or mutilayer film. Another application of TBBT SAMs is to adsorb metal nanoparticles through covalent linkage, forming a strong metal−S bond as shown in Figure 6.

Reactivity of TBBT SAMs on Au with Metal Ions (Cu^{2+}). First, we investigate the reactivity of metal ions with TBBT SAMs, choosing Cu^{2+} as a probe exposing the TBBT SAMs into 1 mM $CuCl_2$ solutions for 10 min. The films obtained were dried in a flow of argon after rinsing with water.

Figure 7 shows the CV curves of Au electrode covered with TBBT SAMs before and after adsorbing Cu(II) ions in 1 M KCl at various scan rates in the range of −200 to +600 mV. In Figure 7, curve a represents TBBT SAMs on Au electrode in 1 M KCl without adsorbing Cu^{2+} ion, demonstrating a behavior of charging capacity. In contrast, when Cu^{2+} ions are adsorbed on TBBT SAMs, a redox couple occurs. The peak current is

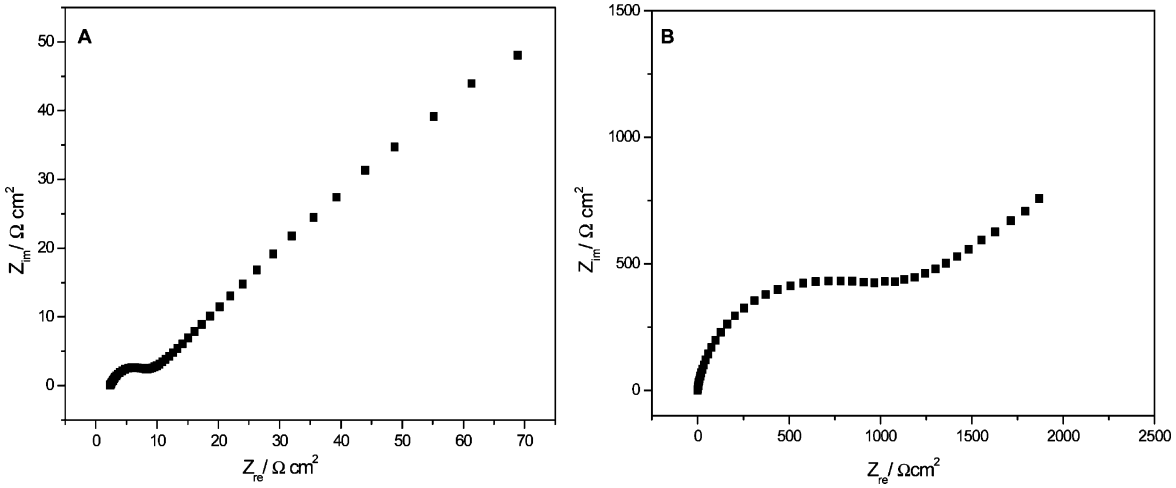

Figure 4. Impedance plot of the bare Au electrode (a) and TBBT on Au electrode (b) in the presence of 5 mM $Fe(CN)_6^{3-/4-}$ with 0.1 M KCl as the supporting electrolyte. The electrode potential was 0.24 V versus Ag/AgCl. The frequency range was 0.01 Hz to 10 kHz.

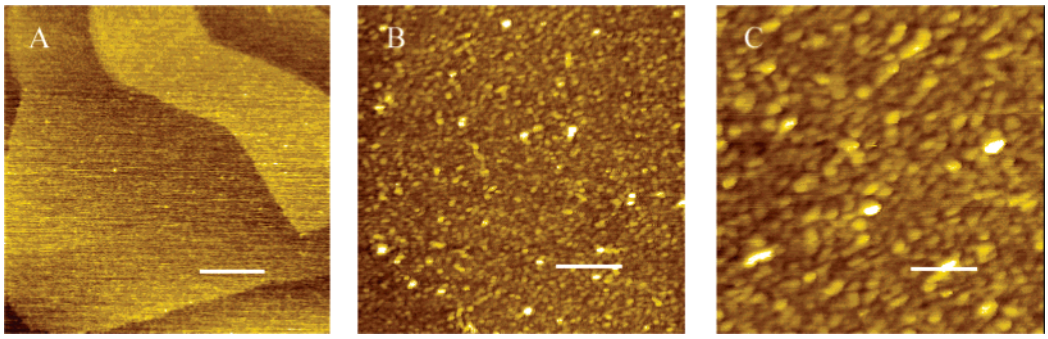

Figure 5. AFM images of (A) Au(111), (B) TBBT SAMs on Au(111) for a 1000 × 1000 nm^2 scan area, and (C) TBBT SAMs on Au(111) for a 500 × 500 nm^2 scan area. The scale bars of (A) and (B) represent 200 nm and and that of (C) is 100 nm.

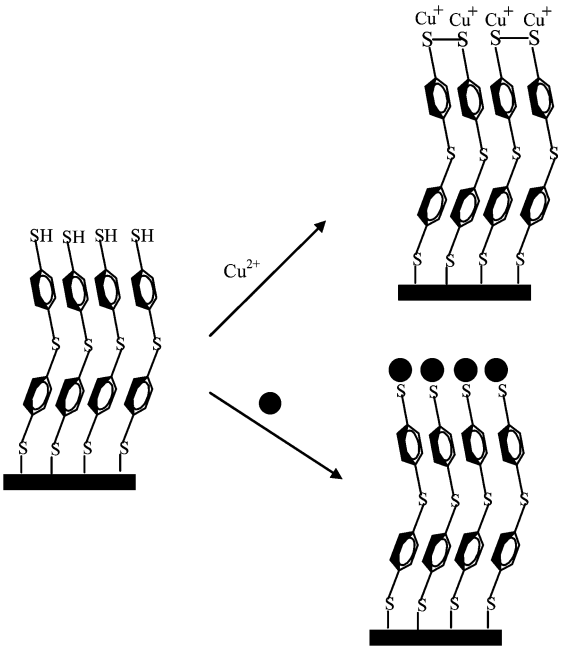

Figure 6. Scheme of TBBT SAMs on Au and its application to react with metal ion (Cu^{2+}) and Ag nanoparticles (●).

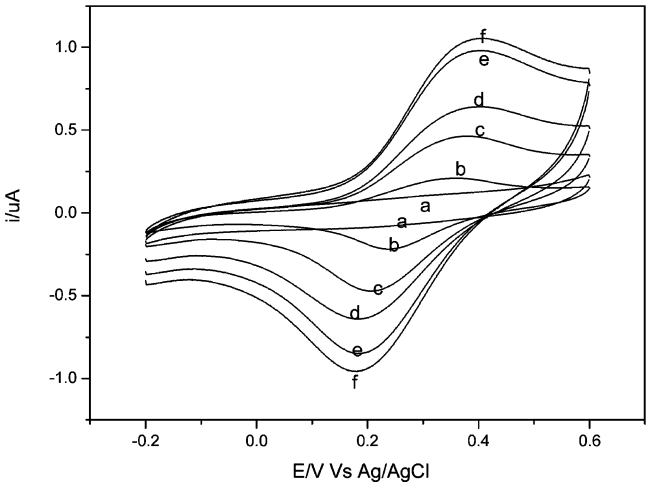

Figure 7. Cyclic voltammograms of Au electrode covered with TBBT SAMs before (a) and after adsorbing Cu(II) ions (from 1 mM aqueous $CuCl_2$ solution) in 1 M KCl at various scan rates: (b) 10, (c) 30, (d) 50, (e) 80, and (f) 100 mV/s.

proportional to the scan rates and the peak separation diminishes with the decrease of scan rates, indicating the surface-confined process of the Cu ion on TBBT SAMs/Au electrode and also suggesting that all adsorbed Cu ions are mostly retained on the SAMs surface. It is noticeable that the voltammetry behavior is quite similar to that reported by Venkataranman et al. and Burst et al. for Cu ions adsorbed on SAMs of 1,4-benzenedimethanethiol in 1 M KCl and 1,6-hexanedithiol in 0.1 M aqueous K_2SO_4,[24c,d] which further illustrates that TBBT SAMs on Au electrode are functionalized by Cu ions.

It is well-known that copper(II) easily oxidizes thiols to disulfides,[25] whether it is in bulk or on the SAM surface;[24] therefore, it is important to clearly learn what is the oxidation state of the adsorbed Cu ion on TBBT SAMs. XPS was conducted on the TBBT SAMs in the S 2p and Cu 2p regions of the bilayer Cu−TBBT SAMs/Au as shown in Figure 8.

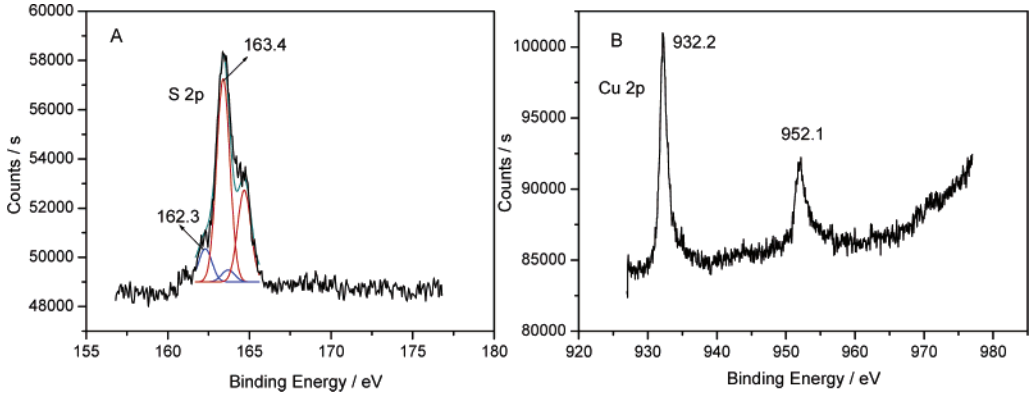

Figure 8. XPS spectra of S 2p (A) and Cu 2p (B) regions of Cu adsorbed on TBBT SAMs/Au.

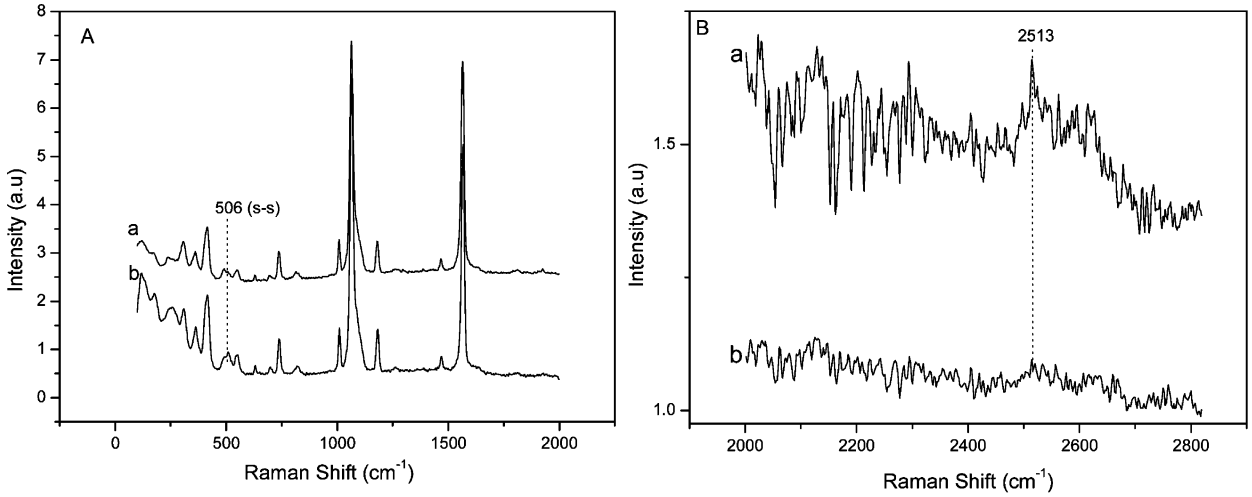

Figure 9. SERS spectra of (a) bare TBBT monolayer on Au and (b) TBBT monolayer exposed to Cu^{2+} ions. (A) Spectra from 100 to 1800 cm^{-1} and (B) the expanded S−H stretching region (from 2200 to 2800 cm^{-1}).

Figure 8A gives the XPS signal of the S peak on Cu-adsorbed TBBT SAMs/Au system. After peak deconvolution, two S 2p (1/2, 3/2) doublets are visible, corresponding to two atomic species, one at an S $2p_{3/2}$ binding energy of 162.3 eV, which can be assigned to thiolate species (Au−S and Cu−S), and another at 163.4 eV, which can be assigned to neutral sulful species (C−S−C).[24a] Peaks at 932.2 (Cu $2p_{3/2}$) and 952.2 eV (Cu $2p_{1/2}$) and the absence of the satellites characteristic of Cu(II) in Figure 8B give clear evidence that Cu is present on the TBBT monolayer as Cu(I), corresponding to the results by Venkataranman et al., who investigated the oxidation state of Cu by electrochemical method.[24c] It should be noted that when the bare gold substrate is immersed in the $CuCl_2$ solution at the same condition, the signal of Cu cannot be detected on the bare gold, indicating that copper is selectively deposited on top of the SAMs.

To more clearly learn the oxidation states of Cu on TBBT SAMs, SERS and electrochemical CV have been conducted on the Cu-adsorbed TBBT SAMs/Au. Figure 9 gives the SERS spectra of TBBT/Au and Cu on TBBT SAMs/Au. A distinct peak at 506 cm^{-1} attributed to the vibration of S−S can be observed clearly, and the vibration of S−H at 2513 cm^{-1} has disappeared completely upon the Cu adsorption on TBBT SAMs as shown in Figure 9B(b), demonstrating that Cu has adsorbed on TBBT SAMs through the Cu−S bond. The formation of S−S indicates that Cu was bound to −SH as monodentate as shown in the scheme of Figure 6, which is similar to the adsorption of Cu on 1,6-hexanedithiol SAMs/Au as reported by Brust.[24d]

Figure 10 gives the voltammetric behavior of the Cu-adsorbed TBBT SAMs/Au system. As shown in Figure 10A, the first anodic sweep gives evidence of oxidation of Cu(I) to Cu(II) at 0.4 V, which confirms that Cu^{2+} ions have been reduced upon adsorption to TBBT SAMs. Other evidence comes from the cathodic sweep carried out toward negative potentials at the first potential sweep as shown in Figure 10B. The dashed curve gives the first potential sweep toward negative potential when the Cu ions adsorbed on TBBT SAMs and no reduction peak can be observed, indicating the initial +1 oxidation state of Cu. In contrast, a distinct peak attributed to the reduction of Cu(II) to Cu(I) as shown in the solid curve of Figure 10B can be observed at 0.18 V when the surface is functionalized by the initial +2 oxidization state of Cu, which further demonstrates the initial +1 oxidation state of Cu on the TBBT SAMs.

Adsorption of Metal Nanoparticles through Covalent Linkage to TBBT SAMs on Au. Another exciting application of SAMs is in the area of nanotechnology, more specifically, the organization of nanoscale particles. Recently, self-assembly of metal nanoparticles into two- (2D) or three-dimensional (3D) nanoarchitecture has attracted more and more attention because of their potential utilization in nanoelectronic devices and surface plasmon resonance (SPR).[26] In our laboratory, CoTMPyP and thionine have been successfully used to fabricate 2D and 3D nanostructures.[27] Herein, it is estimated that metal nanoparticles can be covalently adsorbed on TBBT SAMs to form a layer of metal nanoparticles through the metal−S bond due to the special molecular structure of TBBT SAMs on Au. The covalent attachment of Ag nanoparticles on TBBT SAMs was investi-

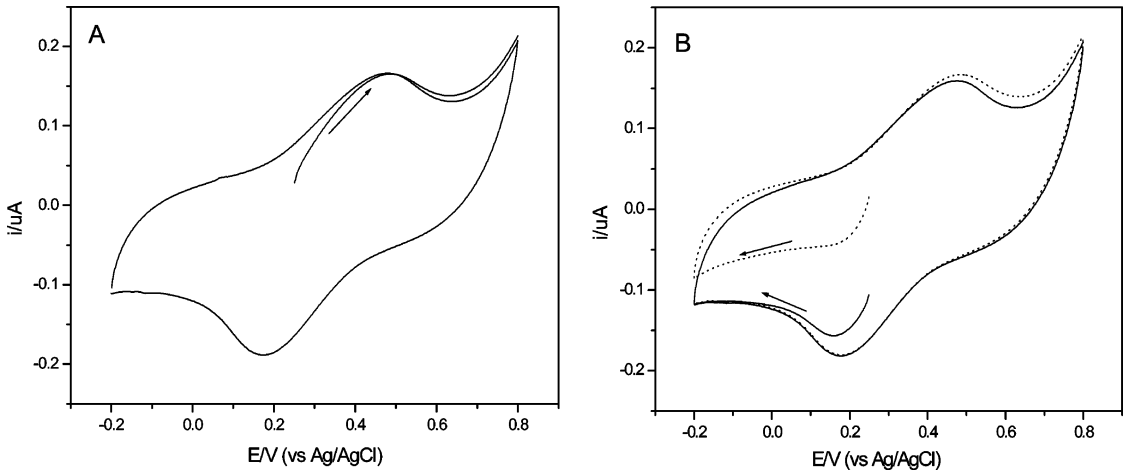

Figure 10. Cyclic voltammogram of Cu ions adsorbed on TBBT SAMs/Au in 1 M KCl. The potential sweep begins at the open-circuit potential of 0.25 V vs Ag/AgCl in the direction of the arrow. (A) The first potential sweep is toward positive potentials. (B) The first potential sweep is toward negative potentials.

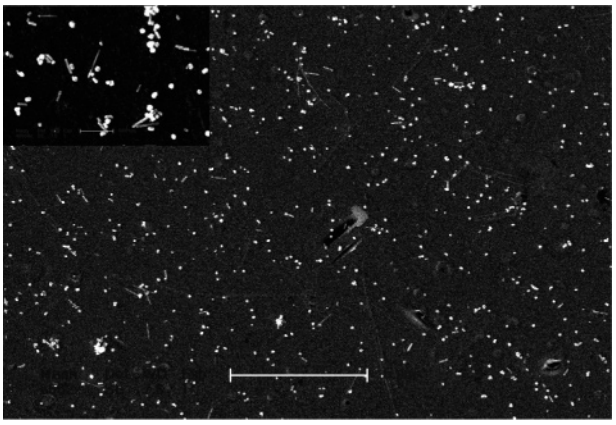

Figure 11. SEM images of Ag nanoparticles on TBBT SAMs/Au. The scale bar represents 5 μm. The inset is the high-magnification SEM image of Ag nanoparticles; the scale bar is 500 nm.

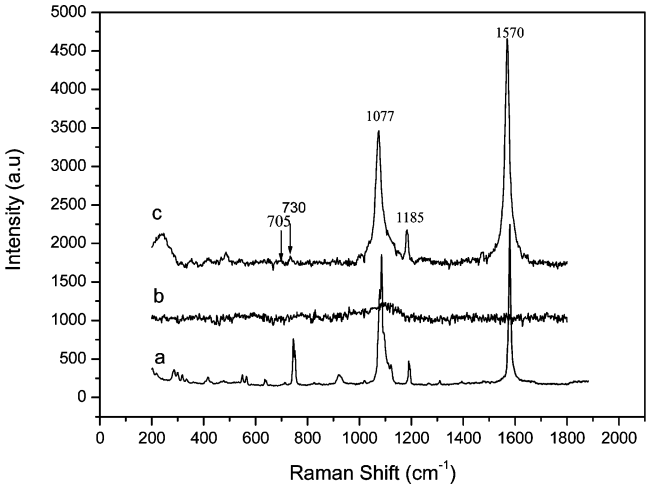

Figure 12. Raman spectra of solid TBBT (a), TBBT on smooth Au (b), and TBBT in smooth macroscopic Au/TBBT SAMs/Ag nanoparticles (c).

gated by immersion in Ag colloid solution for 12 h. Figure 11 shows an SEM image of Ag nanoparticles on TBBT SAMs, in which Ag nanoparticles can be observed clearly to distribute uniformly on TBBT SAMs, though the surface coverage is not high. The high magnification of the SEM image in the inset of Figure 11 gives the size of the Ag nanoparticles as about 75 nm. It should be noted that a few Ag nanorods can also be observed on the SEM images; they are presumed to derive from the Ag colloid formed in synthesis.[16]

Another direct piece of evidence of the Ag nanoparticles adsorbed on the TBBT SAMs is due to the Raman spectrum of TBBT on this structure, as shown in Figure 12. A high-quality Raman spectrum of TBBT is obtained on smooth macroscopic Au/TBBT SAMs/Ag nanoparticles, which can be seen clearly from Figure 12c, compared with the Raman spectra of solid TBBT and TBBT SAMs on smooth Au at 514.5 nm excitation as shown in Figure 12a,b. The vibrations of ν_{C-S} at 1077 cm^{-1} and $\nu_{C-C} + \nu_{C-H}$ at 1570 cm^{-1} are evidently enhanced, which was attributed to the strong electromagnetic coupling of localized surface plasmon (LSP) and surface plasmon polariton (SPP), so-called LSP−SPP.[28] It should be noted that the vibrations due to the stretching and bending modes associated with the CSH have disappeared because of the disruption of S−H bond upon the adsorption of Ag nanoparticles. However, the vibrations associated with CSC groups (705 and 730 cm^{-1}) can be seen in Figure 12c, though very weakly, which was determined by the surface selection rules.[19] Therefore, there is potential for TBBT SAMs on Au to assemble 2D or 3D nanostructures due to the bifunctional properties of TBBT SAMs and their adsorption behavior on Au.

Conclusions

The structure of 4,4′-thiobisbenzenethiol (TBBT) SAMs on Au has been investigated by SERS, electrochemical CV, EIS, and AFM. SERS results indicate TBBT adsorbed on Au surface forming a monolayer, with one of the benzene rings tilted with the surface. In this orientation, one thiol group binds to Au surface as thiolate while the other thiol group is free at the surface of the monolayer. Electrochemical CV and EIS demonstrate there are few pinholes in TBBT SAMs on Au and the coverage fraction (θ) is about 99.6%. AFM provides the detailed surface morphology of the TBBT SAMs on Au. Because of the presence of the free thiol group, it can be used to adsorb Cu^{2+} to form Cu ion functional bilayer films and covalently adsorb Ag nanoparticles. Electrochemical CV, XPS, and SERS results indicate that Cu^{2+} can react with TBBT SAMs and present on TBBT SAMs as Cu(I). SEM image of Ag nanoparticles on TBBT SAMs and Raman spectrum of TBBT on the smooth macroscopic Au/TBBT SAMs/Ag nanoparticles indicate that TBBT SAMs can be used to covalently adsorb metal nanoparticles to form 2D or 3D nanostructures.

Acknowledgment. This work was supported by the National Natural Science Foundation of China (Nos. 20575064, 20427003).

References and Notes

(1) (a) Li, D.; Ratner, M. A.; Marks, T. J.; Zhang, C. H.; Yang, J.; Wong, G. K. *J. Am. Chem. Soc.* **1990**, *112*, 7389. (b) Hickman, J. J.; Ofer, D.; Laibinis, P. E.; Whitesides, G. M. *Science* **1991**, *252*, 688. (c) Venkataramanan, M.; Murty, K. V. G. K.; Pradeep, T.; Deepali, W.; Vijayamohanan, K. *Langmuir* **2000**, *16*, 7673.

(2) Notorya, T.; Poling, Q. W. *Corrosion* **1979**, *35*, 193.

(3) Kaeble, D. H. *Physical Chemistry of Adhesion*; Wiley-Interscience: New York, 1973.

(4) Lopez, G. P.; Biebuyck, H. A.; Harter, R.; Kumor, A.; Whitesides, G. M. *J. Am. Chem. Soc.* **1993**, *115*, 10774.

(5) (a) Bandyopadhyay, K.; Patil, V.; Vijayamohanan, K.; Sastry, M. *Langmuir* **1997**, *13*, 5244. (b) Chumanov, G.; Sokolov, K.; Gregoy, B. W.; Cotton, T. M. *J. Phys. Chem.* **1995**, *99*, 9466. (c) Grabar, K. C.; Freeman, R. G.; Hommer, M. B.; Natan, M. J. *Anal. Chem.* **1995**, *67*, 735. (d) Doron, A.; Katz, E.; Willner, I. *Langmuir* **1995**, *11*, 1313.

(6) (a) Ulman, A. *An Introduction to Ultrathin Organic Films*; Academic Press: Boston, 1991. (b) Dubois, L. H.; Nuzzo, R. G. *Annu. Rev. Phys. Chem.* **1992**, *43*, 437. (c) Laibinis, P. E.; Whitesides, G. M.; Allara, D. L.; Tao, Y. T.; Parikh, A. N.; Nuzzo, R. G. *J. Am. Chem. Soc.* **1991**, *113*, 7152. (d) Ulman, A. *Chem. Rev.* **1996**, *96*, 1533.

(7) (a) Sikes, H. D.; Smalley, J. F.; Dudek, S. P.; Cook, A. R.; Newton, M. D.; Chidsey, C. E. D.; Feldberg, S. W. *Science* **2001**, *291*, 1519. (b) Smalley, J. F.; Sachs, S. B.; Chidsey, C. E. D.; Dudek, S. P.; Sikes, H. D.; Creager, S. E.; Yu, C. J.; Feldberg, S. W.; Newton, M. D. *J. Am. Chem. Soc.* **2004**, *126*, 14620. (c) Adams, D. M.; Brus, L.; Chidsey, C. E. D.; Creager, S.; Creutz, C.; Kagan, C. R.; Kamat, P. V.; Lieberman, M.; Lindsay, S.; Marcus, R. A.; Metzger, R. M.; Michel-Beyerle, M. E.; Miller, J. R.; Newton, M. D.; Rolison, D. R.; Sankey, O.; Schanze, K. S.; Yardley, J.; Zhu, X. *J. Phys. Chem. B* **2003**, *107*, 6668.

(8) Sabatani, E.; Boulakia, J. C.; Bruening, M.; Rubinstein, I. *Langmuir* **1993**, *9*, 2974.

(9) Ganesh, V.; Lakshminarayanan, V. *J. Phys. Chem. B* **2005**, *109*, 16372.

(10) Käfer, D.; Witte, G.; Cyganik, P.; Terfort, A.; Wöll, C. *J. Am. Chem. Soc.* **2006**, *128*, 1723.

(11) (a) Peng, Z. Q.; Dong, S. J. *Langmuir* **2001**, *17*, 4904. (b) Peng, Z. Q.; Tang, J. L.; Han, X. J.; Wang, E. K.; Dong, S. J. *Langmuir* **2002**, *18*, 4834. (c) Peng, Z. Q.; Wang, J. G.; Wang, E. K.; Dong, S. J. *J. Electrochem. Soc.* **2003**, *150*, E197.

(12) (a) Bryant, M. A.; Pemberton, J. E. *J. Am. Chem. Soc.* **1991**, *113*, 3629. (b) Bryant, M. A.; Pemberton, J. E. *J. Am. Chem. Soc.* **1991**, *113*, 8284. (c) Schoenfisch, M. H.; Pemberton, J. E. *J. Am. Chem. Soc.* **1998**, *120*, 4502. (d) Schoenfisch, M. H.; Pemberton, J. E. *Langmuir* **1999**, *15*, 509.

(13) Bryant, M. A.; Joa, S. L.; Pemberton, J. E. *Langmuir* **1992**, *8*, 753.

(14) (a) Lee, T. G.; Kim, K.; Kim, M. S. *J. Phys. Chem.* **1991**, *95*, 9950. (b) Cho, S. H.; Han, H. S.; Jang, D. J.; Kim, K.; Kim, M. S. *J. Phys. Chem.* **1995**, *99*, 10594. (c) Joo, S. W.; Han, S. W.; Kim, K. *J. Phys. Chem. B* **1999**, *103*, 10831. (d) Joo, S. W.; Han, S. W.; Kim, K. *J. Phys. Chem. B* **2000**, *104*, 6218. (e) Joo, S. W.; Han, S. W.; Kim, K. *Langmuir* **2000**, *16*, 5391. (f) Han, S. W.; Lee, S. J.; Kim, K. *Langmuir* **2001**, *17*, 6981.

(15) (a) Liu, Y. C.; Jiang, L. Y. *J. Phys. Chem. B* **2002**, *106*, 6748. (b) Liu, Y. C.; Chuang, T. C. *J. Phys. Chem. B* **2003**, *107*, 12383. (c) Chen, H. J.; Wang, Y. L.; Dong, S. J.; Wang, E. K. *Spectrochim. Acta, Part A* **2005**, *64*, 343.

(16) Lee, P. C.; Meisel, D. *J. Phys. Chem.* **1982**, *86*, 3391.

(17) (a) Frisch, M. J.; Trucks, G. W.; Schlegel, H. B.; Scuseria, G. E.; Robb, M. A.; Cheeseman, J. R.; Montgomery, J. A., Jr.; Vreven, T.; Kudin, K. N.; Burant, J. C.; Millam, J. M.; Iyengar, S. S.; Tomasi, J.; Barone, V.; Mennucci, B.; Cossi, M.; Scalmani, G.; Rega, N.; Petersson, G. A.; Nakatsuji, H.; Hada, M.; Ehara, M.; Toyota, K.; Fukuda, R.; Hasegawa, J.; Ishida, M.; Nakajima, T.; Honda, Y.; Kitao, O.; Nakai, H.; Klene, M.; Li, X.; Knox, J. E.; Hratchian, H. P.; Cross, J. B.; Bakken, V.; Adamo, C.; Jaramillo, J.; Gomperts, R.; Stratmann, R. E.; Yazyev, O.; Austin, A. J.; Cammi, R.; Pomelli, C.; Ochterski, J. W.; Ayala, P. Y.; Morokuma, K.; Voth, G. A.; Salvador, P.; Dannenberg, J. J.; Zakrzewski, V. G.; Dapprich, S.; Daniels, A. D.; Strain, M. C.; Farkas, O.; Malick, D. K.; Rabuck, A. D.; Raghavachari, K.; Foresman, J. B.; Ortiz, J. V.; Cui, Q.; Baboul, A. G.; Clifford, S.; Cioslowski, J.; Stefanov, B. B.; Liu, G.; Liashenko, A.; Piskorz, P.; Komaromi, I.; Martin, R. L.; Fox, D. J.; Keith, T.; Al-Laham, M. A.; Peng, C. Y.; Nanayakkara, A.; Challacombe, M.; Gill, P. M. W.; Johnson, B.; Chen, W.; Wong, M. W.; Gonzalez, C.; Pople, J. A. *Gaussian 03*, revision C.02; Gaussian, Inc.: Wallingford, CT, 2004. (b) Petersson, G. A.; Bennett, A.; Tensfeldt, T. G.; Al-Laham, M. A.; Shirley, W. A.; Mantzauis, J. *J. Chem. Phys.* **1988**, *89*, 2163

(18) (a) Santos, E.; Schurrer, C.; Brunetti, A.; Schmickler, W. *Langmuir* **2002**, *18*, 2771. (b) Sellers, H.; Ulman, A.; Shnidam, Y.; Eilers, J. E. *J. Am. Chem. Soc.* **1993**, *115*, 9389.

(19) (a) Moskovits, M. *Rev. Mod. Phys.* **1985**, *57*, 783. (b) Otta, A.; Mrozek, I.; Grabhorn, H.; Akemann, W. *J. Phys.: Condens. Matter Phys.* **1992**, *4*, 1143. (c) Jung, H. H.; Won, D. Y.; Shin, S.; Kim, K. *Langmuir* **1999**, *15*, 1147.

(20) (a) Joo, T. H.; Yim, Y. H.; Kim, K.; Kim, M. S. *J. Phys. Chem.* **1989**, *93*, 1422. (b) Yim, Y. H.; Kim, K.; Kim, M. S. *J. Phys. Chem.* **1990**, *94*, 2552. (c) Lee, I.; Han, S. W.; Kim, C. H.; Kim, T. G.; Joo, S. W.; Jang, D. J.; Kim, K. *Langmuir* **2000**, *16*, 9963. (d) Kim, K. L.; Lee, S. J.; Kim, K. *J. Phys. Chem. B* **2004**, *108*, 9216.

(21) Bard, A. J.; Faulkner, L. R. *Electrochemical Methods. Fundamentals and Applications*; Wiley: New York, 2003.

(22) Janek, R. P.; Fawcett, W. R.; Ulman, A. *Langmuir* **1998**, *14*, 3011.

(23) (a) Sabatani, E.; Rubinstein, I.; Maoz, R.; Sagiv, J. *J. Electroanal. Chem.* **1987**, *219*, 365. (b) Sabatani, E.; Rubinstein, I. *J. Phys. Chem.* **1987**, *91*, 6663.

(24) (a) Brower, T. L.; Garno, J. C.; Ulman, A.; Liu, G. Y.; Yan, C.; Golzhauser, A.; Grunze, M. *Langmuir* **2002**, *18*, 6207. (b) Kang, J. F.; Ulman, A.; Liao, S.; Jordan, R.; Yang, G. H.; Liu, G. Y. *Langmuir* **2001**, *17*, 95. (c) Venkataramanan, M.; Murty, K. V. G. K.; Pradeep, T.; Deepali, W.; Vijayamohanan, K. *Langmuir* **2000**, *16*, 7673. (d) Brust, M.; Blass, P. M.; Bard, A. J. *Langmuir* **1997**, *13*, 5602.

(25) (a) Evans, S. D.; Ulman, A.; Goppert-Berarducci, K. E.; Gerenser, L. J. *J. Am. Chem. Soc.* **1991**, *113*, 5866. (b) Michaelis, L.; Schubert, M. P. *J. Am. Chem. Soc.* **1930**, *52*, 4418.

(26) (a) Ball, P. *Nature* **1993**, *362*, 123. (b) Ashwell, G. J. *Molecular Electronics*; Wiley: New York, 1992.

(27) (a) Cheng, W.; Dong, S.; Wang, E. *J. Phys. Chem. B* **2004**, *108*, 19146. (b) Cheng, W. L.; Jiang, J. G.; Dong, S. J.; Wang, E. K. *Chem. Commun.* **2002**, *16*, 1706.

(28) (a) Zheng, J. W.; Zhou, Y. G.; Li, X. W.; Ji, Y.; Lu, T. H.; Gu, R. A. *Langmuir* **2003**, *19*, 632. (b) Orendorff, C. J.; Gole, A.; Sau, T. K.; Murphy, C. J. *Anal. Chem.* **2005**, *77*, 3261.